Published in final edited form as:
Inorg Chem. 2011 January 17; 50(2): 427–436. doi:10.1021/ic1006378.

S K-edge XAS and DFT Studies of High and Low Spin {FeNO}^{7} Thiolate Complexes: Exchange Stabilization of Electron Delocalization in {FeNO}^{7} and {FeO$_2$}^{8}

Ning Sun[1], **Lei V. Liu**[1], **Abhishek Dey**[1,2], **Gloria Villar-Acevedo**[3], **Julie A. Kovacs**[3], **Marcetta Y. Darensbourg**[4], **Keith O. Hodgson**[1,5], **Britt Hedman**[5], and **Edward I. Solomon**[1,5]

Edward I. Solomon: edward.solomon@stanford.edu

[1]Department of Chemistry, Stanford University, Stanford, California 94305

[3]Department of Chemistry, University of Washington, Seattle, Washington 98195

[4]Department of Chemistry, Texas A&M University, College Station, Texas 77843

[5]Stanford Synchrotron Radiation Lightsource, SLAC, Stanford University, Menlo Park, California 94025

Abstract

S K-edge XAS is a direct experimental probe of metal ion electronic structure as the pre-edge energy reflects its oxidation state, and the energy splitting pattern of the pre-edge transitions reflects its spin state. The combination of sulfur K-edge XAS and DFT calculations indicates that the electronic structures of {FeNO}^{7} (S=3/2) ($S^{Me2}N_4$(tren)Fe(NO), complex I) and {FeNO}^{7} (S=1/2) ((bme-daco)Fe(NO), complex II) are Fe^{III}(S=5/2)-NO^-(S=1) and Fe^{III}(S=3/2)-NO^-(S=1), respectively. When an axial ligand is computationally added to complex II, the electronic structure becomes Fe^{II}(S=0)-NO• (S=1/2). These studies demonstrate how the ligand field of the Fe center defines its spin state and thus changes the electron exchange, an important factor in determining the electron distribution over {FeNO}^{7} and {FeO$_2$}^{8} sites.

Introduction

Mononuclear non-heme iron centers are present in a wide range of enzymes that carry out reactions involved in oxygen activation.[1], [2] To obtain molecular insight into the mechanisms of these enzymes, it is important to have a detailed description of the electronic structure of the non-heme iron-dioxygen adducts.[3] However, these oxygen intermediates often rapidly react and are therefore not amenable to experimental study. NO has been shown to reversibly bind to the ferrous center of many mononuclear non-heme iron enzymes and model complexes, forming stable Fe-NO complexes that can be spectroscopically studied.[4]-[9] These Fe-NO complexes can serve as analogs of dioxygen intermediates and provide insight into the electronic structures of the intermediates and the mechanisms of oxygen activation.[3], [10], [11] In addition to being an analog, non-heme Fe-NO complexes are active in biological processes such as the nitric oxide reductases[12].

Correspondence to: Keith O. Hodgson; Britt Hedman; Edward I. Solomon, edward.solomon@stanford.edu.

[2]The current address is Department of Inorganic Chemistry, Indian Association for the Cultivation of Science, Kolkata, India 700032.

Supporting Information **Available:** The determination of effective nuclear charge, the complete reference for Gaussian 03 and Gaussian09, the MO compositions of complex II using different basis sets, the MO compositions of model A and C, the occupied MO diagrams and the optimized geometries for complex I, II, and II + axial L. This material is available free of charge via the Internet at http://pubs.acs.org.

The Fe-NO complexes considered here are of the $\{FeNO\}^7$ type according to the Enemark and Feltham notation,[13] i.e. the total number of valence electrons in the Fe d and NO π* orbitals is seven. The spin state of these $\{FeNO\}^7$ complexes is either S=3/2 or S=1/2. The electronic structures of $\{FeNO\}^7$ complexes have been controversial.[3, 6-8, 10, 11, 14-31] Plausible descriptions are presented in Scheme 1A and 1B. For $\{FeNO\}^7$(S=3/2), reference 11 presented spectroscopic evidence and calculations which strongly support an electronic description of a high spin Fe^{III} (S=5/2) antiferromagnetically coupled to NO^- (S=1). For $\{FeNO\}^7$(S=1/2), a number of studies[7, 17-20] invoke a description of low spin Fe^{II} (S=0) coupled to NO•(S=1/2), while references 21 and 24 proposed a description of intermediate spin Fe^{III} (S=3/2) antiferromagnetically coupled to NO^- (S=1).

We have developed sulfur K-edge X-ray absorption spectroscopy (XAS) as a direct experimental probe of the electronic structure and bonding in metal complexes.[32-34] The K-edge X-ray absorption spectrum of a sulfur ligand bound to a transition metal ion can have an intense pre-edge feature, which is assigned as a sulfur 1s to metal 3d transition. The intensity of this transition (i.e. $I(S_{1s} \rightarrow \Psi^*_d)$ in eq. 1, below) is directly proportional to the % sulfur np character (α^2) mixed into unoccupied or half-occupied valence metal d orbitals $\Psi^*_d = (1-\alpha^2)^{1/2}|M_d> - \alpha|S_{3p}>$ of a transition metal complex.[32, 35]

$$I(S_{1s} \rightarrow \Psi^*_d) = \alpha^2 I(S_{1s} \rightarrow S_{3p}) \quad (1)$$

Here $I(S_{1s} \rightarrow S_{3p})$ is the intrinsic intensity of a sulfur 1s→3p transition. Thus the pre-edge intensity provides a direct measure of sulfur-metal bond covalency (α^2).

The energy of the pre-edge transition reflects the energy difference between the metal d and sulfur 1s orbital. For the same type of sulfur ligand (i.e. thiolate, sulfide, dithiolene) the energy of the sulfur 1s orbitals is fairly constant[34]. Therefore, the pre-edge energy reflects the energy of the metal d electron acceptor orbital, which is dependent on the ligand field and, more strongly, the effective nuclear charge (Z_{eff}) of the metal, which in turn is determined by its oxidation state. In addition, the pre-edge energy splitting pattern reflects the half-occupied and unoccupied d orbitals, hence the spin state of the metal center.[36] Therefore, S K-edge XAS is a direct experimental probe of metal ion electronic structure.

In the present study, ($S^{Me2}N_4$(tren))Fe(NO) (complex I, S=3/2 determined by EPR and SQUID)[37] and (bme-daco)Fe(NO) (complex II, S=1/2 determined by EPR)[38] are examined since complex I is an SOR (superoxide reductase) analog while complex II is the only reported $\{FeNO\}^7$ (S=1/2) model complex that contains sulfur ligands. Both complexes are structurally defined by x-ray crystallography and have a bent Fe-N-O unit. (The structures are shown in Figure 1; bond lengths and angles are given in Table 1.) Complex I is six-coordinate with one thiolate, one imine and three amine ligands while complex II is a five-coordinate complex with two thiolate ligands and two amine ligands, in addition to the NO moiety.

A combination of sulfur K-edge XAS and DFT calculations is used to elucidate the electronic structures of $\{FeNO\}^7$(S=3/2) (complex I) and $\{FeNO\}^7$(S=1/2) (complex II). The experimentally validated computational results are further used to explore the factors determining the electron distribution over the $\{FeNO\}^7$ unit. These studies are also relevant to $\{FeO_2\}^8$ intermediates (see Discussion) as they demonstrate how the metal ion spin state (a result of its ligand field) influences the electron distribution over FeNO and FeO_2 sites.

Experimental Details

Sample preparation

The complexes ($S^{Me2}N_4$(tren))Fe(NO) and (bme-daco)Fe(NO) were synthesized according to procedures in the literature.[37-40] For complex I, SQUID data gave a good fit (R^2=0.999) over the temperature range T = 5 - 265 K, with μ_{eff}=4.12 BM, and the elemental analysis of the solid isolated compound is good (Anal. Calcd for $FeC_{35}H_{43}N_5O_1S_1$: C, 64.74%, H, 6.62%; N, 10.79%. Found: C, 64.67%; H, 6.53%; N, 10.29%). Spin quantitation of the EPR signal (vs Fe^{III}EDTA) indicated 96% purity.[37] For complex II, the samples studied were in pure crystalline form (ground into powder). The analytical data for the crystals can be found in [ref 38]. For S K-edge XAS experiments, the samples were ground into a fine powder and dispersed as thinly as possible on sulfur-free Mylar tape in a N_2-filled inert atmosphere glovebox. This procedure has been verified to minimize self-absorption effects. The samples were then mounted across the window of a 1 mm thick aluminum plate. A 6.3 μm polypropylene film window protected the solid samples from exposure to air during transfer from the glovebox to the experimental sample chamber.

Data Collection and Analysis

All sulfur K-edge data were measured at the Stanford Synchrotron Radiation Lightsource using the 54-pole wiggler beam line 6-2 under ring conditions of 3 GeV and 60–100 mA. Details of the experimental configuration for low-energy studies have been described previously.[34] The photon energy was calibrated to the maximum of the first pre-edge feature of $Na_2S_2O_3$•$5H_2O$ at 2472.02 eV. A total of 3-5 scans were measured per sample to ensure reproducibility. Raw data were calibrated and averaged using EXAFSPAK.[41] Using the PySpline program,[42] the background was removed from all spectra by fitting a second-order polynomial to the pre-edge region and subtracting it from the entire spectrum. Normalization of the data was accomplished by fitting a flat second-order polynomial or straight line to the post-edge region and normalizing the edge jump to 1.0 at 2490 eV. The intensities of the pre-edge features were quantified by fitting the data with pseudo-Voigt line shapes with a fixed 1:1 ratio of Lorentzian to Gaussian contributions, using the EDG_FIT program.[41] The reported intensity values are based on the average of 10-12 good fits. In addition to the error resulting from the background correction and fitting procedure (∼2%), normalization procedures can introduce 1-3% error in the total pre-edge peak areas. The uncertainty in pre-edge energy is ∼0.1 eV.[43]

DFT Calculations

Geometry optimization and single point calculations were performed on dual-CPU Intel Xeon workstations using the Gaussian 03 package.[44] The optimizations were performed using the unrestricted B3LYP hybrid functional[45, 46] for both complexes. For complex I, the 6-311+G(3df) basis set was used for Fe, S, N, and O atoms and 6-311+G* was used for C and H atoms. For complex II, the 6-311+G* basis set was used for Fe, S, N, and O atoms and 6-311G* was used for C and H atoms[47]. The initial coordinates for the geometry optimization were obtained from the crystal structures.[37, 38] Single point calculations were performed for both complexes using the unrestricted B3LYP functional and a 6-311+G(3df) basis set on the Fe, S, N, and O atoms and a 6-311+G* basis set on the C and H atoms with tight convergence. The molecular orbitals were plotted using the Gaussview v.3.0 software, and Mulliken population analyses[48-51] were performed using the QMForge program.[52] TD-DFT calculations were performed with the electronic structure program ORCA[53, 54] with the same basis sets and functional as the single point calculations. The $\{FeO_2\}^8$ complexes in different configurations were calculated using the Gaussian 09 package.[55]

Results

A. S K-Edge X-ray Absorption Spectroscopy

The S K-edge XAS data for ($S^{Me2}N_4$(tren))Fe(NO) (complex I, S=3/2, blue) and (bme-daco)Fe(NO) (complex II, S=1/2, green) are presented in Figure 2. The resolved pre-edge fits are shown on an expanded scale in Figure 3, with fit results given in Table 2. Complex I shows two pre-edge features, at 2470.1 eV and 2471.0 eV, respectively, split by 0.9 eV. Complex II also shows two pre-edge features, at 2470.5 eV and 2471.6 eV, split by 1.1 eV with a different intensity pattern.

To elucidate the electronic structures of complex I and II, data of three reference complexes are also included in Figure 2. Fe^{III}($S^{Me2}N_4$(tren))(NCS) (black) is a six-coordinate low spin ferric complex[56] which shows three pre-edge features associated with transitions to $^1A_1$, to $^3T_1$, $^3T_2$ and $^1T_1$, and to $^1T_2$ states, respectively[57] (vertical lines in Figure 2); Fe^{III}-SOR (red) is a six-coordinate high spin ferric protein site, which has two pre-edge features of comparable intensity, assigned to S 1s→Fe d(t_2) and S 1s→Fe d(e)[58] transitions; Fe^{II}-SOR (light blue) is a six-coordinate high spin ferrous complex, whose pre-edge feature is higher in energy and obscured by the S 1s transition to the S-C σ* orbital at ∼2472.5 eV.[58]

Both complex I and complex II show distinct pre-edge features in the same energy region as the Fe^{III} reference complexes, showing that their Z_{eff} reflects an Fe^{III} site. The shape of the complex I pre-edge feature (blue in Figure 2) resembles that of Fe^{III}-SOR (red, two peaks of comparable intensity split by ∼1.2eV), suggesting that complex I is a high spin Fe^{III} complex. However, the pre-edge feature of complex II (i.e. two peaks with intensity ratio of 2.5 : 1, split by ∼1.1 eV) differs from that of Fe^{III}-SOR as well as from that of the low spin reference complex Fe^{III}($S^{Me2}N_4$(tren))(NCS) (black in Figure 2), which shows three pre-edge features (with the intensity ratio of 1.1 : 4.8 : 1). This indicates that while complex II has an Fe^{III} site, it is neither high nor low spin, raising the possibility of an intermediate spin ground state. This is supported by TD-DFT calculations in section B.

Since there is a linear relationship between oxidation state and effective nuclear charge[59], and the pre-edge transition energy reflects the Z_{eff} (for the same type of S ligand), we can estimate the oxidation states of the iron in complex I and II based on their pre-edge transition energies relative to those of the Fe^{III}SOR and Fe^{II}SOR references[60]. Using the Slater-Zener rules,[59], [61] the oxidation state is estimated to be 2.75 for complex I and 2.67 for complex II (see Supporting Information). These results indicate that both complexes I and II have oxidation states close to the oxidation state of the Fe^{III} reference complex defined as 3.0.

B. DFT Modeling

Geometry optimizations were performed using the spin unrestricted B3LYP functional, starting from the crystal structures[37], [38] for both complexes. The optimized geometric parameters for complexes I and II are listed in Table 1 for comparison to the parameters from the crystal structures. For both complexes, the optimized bond lengths and angles agree well with those of the crystal structures, with the main differences being that for complex I the calculated Fe-amine bond lengths are longer than in the crystal structure by ∼0.1 Å and for complex II the O-N-Fe-S dihedral angle is calculated to be larger than in the crystal structure. However, the total energy change is only 0.56 kcal/mol for the bond length change in complex I and 0.13 kcal/mol for the angle change in complex II relative to the crystallographic values.

The calculated wavefunctions for both complexes were found to be stable using the stability check option in Gaussian 03. From the Mulliken spin densities[50] in Table 1, both complexes are determined to have the Fe and NO antiferromagnetically coupled.

The calculated MO diagrams for both complexes are presented in Figure 4A and B. Only the lowest seven unoccupied orbitals that have significant Fe d or NO π* character are included in the diagram and are analyzed further.[62] From the MO diagram, complex I has two unoccupied alpha orbitals that are composed mainly of NO π* character (π_h* denotes the orbital in the Fe-N-O plane; π_v*denotes the orbital perpendicular to the Fe-N-O plane) and five unoccupied beta orbitals that are composed mainly of Fe d character. Complex II has three alpha and four beta unoccupied orbitals, all of which have both Fe and NO character. Two alpha orbitals are mainly NO π*, while one alpha and the four beta orbitals are mainly Fe d.

Total S covalencies were calculated by summing the S p component in the orbitals shown in the MO diagram. The calculated S covalencies are listed in Table 1 (bottom). For both complexes, the calculated total S covalencies are lower than the experimental values from S K-edge XAS in Table 2 by 4% for complex I and 15% for complex II.[63]

To further test the results of these electronic structure calculations, TD-DFT calculations were performed to simulate the S K-edge XAS data. In Figure 5 the energy is shifted up by 57.3 eV to compensate for relativistic effects that are not included in the calculation and the intensity is scaled down by 0.024 to compensate for the intensity normalization of the experimental data.[64] For both complexes, the calculated S K-edge XAS spectra reproduce the split pre-edge in the experimental spectra, supporting the accuracy of the calculated descriptions of the bonding. From these TD-DFT calculations, for complex I (Figure 5A) the pre-edge feature at 2470.1 eV is assigned to transitions to the Fe t_2 (β) orbitals (d_{yz} (87β), d_{xy} (88β), and d_{xz} (89β)) and that at 2471.0 eV is assigned to transitions to Fe e (β) (d_{x2-y2} (90β) and d_{z2} (91β)) and NO π* (α) (90,91α) orbitals. For complex II the pre-edge feature at 2470.5 eV is assigned as transitions to Fe d_{xz} (β) (84β), d_{yz} (β) (85β), d_{z2} (β) (86β) and d_{x2-y2} (α) (85α) orbitals[65] while that at 2471.6 eV has contributions from the transitions to Fe d_{x2-y2} (β) (87β) and NO π* (α) (86,87α) orbitals.

Analysis

A. Electronic Structure of Complex I (S=3/2)

For complex I $\{FeNO\}^7$ (S=3/2) in Figure 4A, the two unoccupied α orbitals 90 and 91 are NO π* orbitals and the five unoccupied β orbitals 87-91 all have dominant Fe d character, i.e. the Fe d orbitals have five α electrons while the NO π* orbitals have two beta electrons. Therefore, complex I is described as a high spin Fe^{III} (S=5/2) antiferromagnetically coupled to triplet NO^- (S=1) (Scheme 2, left). This is electronic description is consistent with the experimental S K-edge XAS result that complex I has a high spin ferric center very similar to that in Fe^{III}-SOR. It is also consistent with our earlier studies.[3, 11]

We also note that the wavefunctions in Figure 4A are significantly delocalized between the Fe d orbitals (especially d_{xz} and d_{yz}) and the NO π* orbitals. The delocalization in the β unoccupied orbitals between d_{xz} and NO π_h* and between d_{yz} and NO π_v* reflects the amount of electron donation from the occupied NO^- π* to the Fe d orbital while the delocalization in the α unoccupied orbitals between NO π* and d_{xz}/d_{yz} reflects the backbonding of the occupied Fe d character into the NO π* orbitals. Because the amount of electron donation from NO π* to Fe d (total ~66%) is much larger than that from Fe to NO (total ~9%), the net delocalization somewhat decreases the Z_{eff} of the Fe^{III} center. This is consistent with the fact that the oxidation state estimated from S K-edge data is 2.75, which

is lower than the oxidation state of the Fe^{III}-SOR reference complex of 3. Rodriguez et al.[14] have drawn a similar conclusion from the isomer shifts in the Mössbauer spectra and from DFT calculations for nitrosyl derivatives of deoxy hemerythrin.

B. Electronic Structure of Complex II (S=1/2)

For complex II, the MO diagram in Figure 4B shows that there are two α holes in NO π* (86, 87) and one α (85) and four β holes (84-87) in Fe d orbitals, i.e. the Fe d orbitals have four α electrons and one β electron while the NO π* orbitals have two β electrons. Therefore, complex II is described as an intermediate spin Fe^{III}(S=3/2) antiferromagnetically coupled to triplet NO^-(S=1) (Scheme 2, middle left). This description is consistent with the experimental results from the S K-edge data that complex II has an intermediate spin ferric center.

Complex II also has the seven valence electrons partially delocalized within the {FeNO} unit. The electron delocalization of the four unoccupied β orbitals reflects the amount of electron donation from the NO π* into the Fe d orbitals (~60% total), while the delocalization of the unoccupied α orbitals 86 and 87 reflects the backbonding from the occupied Fe d_{xz}/d_{yz} into the NO π_h^*/π_v^* orbitals (~15% total). As in complex I, the net NO^- donation in complex II decreases the Z_{eff} of the Fe^{III} center. This is consistent with the Z_{eff} estimated from the S K-edge data, that it is lower in complex II relative to the Fe^{III}-SOR reference.[66]

C. Correlation of the Electronic Structure Description of Complex II (S=1/2) to Descriptions in the Literature

From the S K-edge XAS spectra and DFT calculations, complex II is described as Fe^{III}(S=3/2)-NO^-(S=1) S=1/2, i.e. an intermediate spin state ferric center antiferromagnetically coupled to a triplet NO^-. However, in the literature, most {FeNO}^{7}(S=1/2) complexes have been described as Fe^{II}(S=0)-NO•(S=1/2), i.e. a low spin ferrous center coupled to a NO radical[7, 17-20], with the exception of reference 21 and 24, in which an Fe^{III}(S=3/2)-NO^-(S=1) description is proposed.

There are two possible explanations for this discrepancy: 1) the method used here to determine the electronic structure is different from that used in the literature; 2) the electronic structure of complex II is different from that of the other complexes studied, reflecting its different geometric structure. The first possibility can be ruled out because B3LYP was also used in the previous studies[7, 17, 18, 20] and the description of complex II does not change when the basis sets used in literature were examined (See Table S1), indicating that the electronic structure difference may be due to the specific geometric structure of complex II.

The structure of complex II is different from the structures in the literature[7, 17-20] in two ways: 1) there are two *cis* thiolate ligands; 2) complex II is five-coordinate with a pseudo-square pyramidal geometry (similar to the complex in reference 24) while the other complexes in the literature all have six ligands and are pseudo-octahedral. To investigate the effects of these structural differences, we performed calculations on three models: A) the thiolate ligands in complex II were replaced by amines; B) a N coordinated axial CN^- ligand was added to the original structure, *trans* to the NO; C) the thiolate ligands were replaced by amines and an axially N-coordinated CN^- ligand was added.

From the calculations (Table S2 and S3), model A gives the same electronic structure description as the original structure of complex II (Fe^{III}(S=3/2)-NO^-(S=1)) while models B and C both give a low spin ferrous (S=0) center coupled to an NO radical (Scheme 2 right),

equivalent to most of the descriptions in the literature. The MO diagram for complex II + axial L is given in Figure 4C. There are two α and two β holes in the d σ orbitals (i.e. a $(t_{2g})^6$ configuration on the Fe) and one α and two β holes in the NO π* orbitals (i.e. an NO• configuration). These results indicate that it is the lack of an axial ligand that changes the electronic structure of complex II relative to that of most of the complexes studied previously.

D. Ligand Field Contributions to Spin States of {FeNO}^{7}

It is interesting that in going from complex I to complex II to complex II + axial L, the {FeNO}^{7} moiety changes from Fe^{III}(S=5/2)-NO^-(S=1) to Fe^{III}(S=3/2)-NO^-(S=1) to Fe^{II}(S=0)-NO•(S=1/2). From the analysis in section C, the ligand field of the Fe can affect its spin state and thus the electronic structure of the {FeNO}^{7} site.

From the MO diagrams in Figure 4, complex I has a high spin ferric center with one α electron in each d orbital, while complex II has an intermediate spin ferric center with an electron pair in the d_{xy} orbital and an unoccupied d_{x2-y2} orbital. The Fe^{III} center in complex II is intermediate spin rather than high spin because the energy gap between the d_{x2-y2} and d_{xy} orbitals is large enough to overcome the electron repulsion increase associated with electron pairing in the d_{xy} orbital. From DFT calculations, the energy difference between the d_{x2-y2} and d_{xy} orbitals in complex I is 1.2 eV while the energy difference between d_{x2-y2} and d_{xy} in complex II is 2.3 eV[67]. This large energy gap between d_{x2-y2} and d_{xy} orbitals in complex II reflects its square pyramidal geometry with stronger σ donating equatorial ligands (Figure 6).

When the axial ligand is computationally added to complex II, the ligand field along the *z* axis becomes stronger and shifts the d_{z2} orbital higher in energy. This would result in a shift of the d_{z2} electron of complex II into the d_{xz} orbital to spin pair, producing a low spin Fe^{III} state (Scheme 2 center-right). However, the computed electronic structure description of complex II + axial L is a low spin Fe^{II}. This means that upon going low spin due to the strength of the ligand field, one electron also transfers from the NO^- π_v* orbital into the Fe d_{yz} orbital, resulting in a low spin Fe^{II} and NO• (Scheme 2, far right). The driving force for this electron transfer is investigated below.

E. Exchange Contributions to the Electron Distribution over {FeNO}^{7}

Normally adding an axial ligand would stabilize the oxidized Fe^{III} state, however, the computed electronic structure for complex II + axial L is Fe^{II}-NO•. This indicates that the total energy of the Fe^{II}-NO• configuration is lower than that of the Fe^{III}-NO^- configuration, i.e. the total energy change in going from Fe^{III}-NO^- to Fe^{II}-NO• (ΔE_{tot}) is negative for complex II + axial ligand. In contrast, for complex II (without an axial ligand), ΔE_{tot} is positive since the ground state is Fe^{III}-NO^-.

In going from the Fe^{III}-NO^- to the Fe^{II}-NO• configuration for complex II (Scheme 3 left half) and complex II+axial L (scheme 3 right half) an electron is transferred from the NO π* orbital to the acceptor Fe d orbital. Since the NO π* orbital is higher in energy than the Fe d orbital in both complexes, the Fe^{II}-NO• configuration is favored (i.e. the one electron orbital energy difference, ΔE_{orb}, is negative). Since there is one more donor ligand on the Fe in complex II + axial L, the Z_{eff}^{Fe} is less positive and the d manifold should be higher in energy, its ΔE_{orb} should be less negative. Therefore, this term will stabilize Fe^{II}-NO• configuration more in complex II than in complex II + axial L, the reverse of what is found in the DFT calculations and experiments for complex II.

However, two additional contributions have to be considered in evaluating the relative stability of the two electronic configurations for the two complexes: 1) the decrease in the stabilization energy due to the antiferromagnetic exchange coupling between the spins on the Fe and NO, ΔE_{AF}, and 2) differences in the e^--e^- repulsion interaction between the two configurations for each of the two complexes, ΔE_{repl}.

1) ΔE_{AF}—This term has an energy contribution to the stabilization of the ground state of each configuration for each complex in Scheme 3, which is given by equation 2 (for $\mathbf{H} = -2J\mathbf{S}_1 \bullet \mathbf{S}_2$, where J is the antiferromagnetic exchange coupling constant):

$$E_{AF} = -J(S_{tot}(S_{tot}+1) - S_1(S_1+1) - S_2(S_2+1). \quad (2)$$

For complex II, the Fe^{III}(S=3/2)-NO^-(S=1) S_{tot}=1/2 configuration has E_{AF} of 5J, the Fe^{II}(S=1)-NO•(S=1/2) S_{tot}=1/2 configuration has E_{AF} of 2J and thus ΔE_{AF}=-3J, assuming similar J values for both configurations. For complex II + axial L (Scheme 3 right half), the Fe^{III}(S=1/2)-NO^-(S=1) S_{tot}=1/2 configuration is stabilized by 2J while the Fe^{II}(S=0)-NO•(S=1/2) S_{tot}=1/2 configuration has no exchange stabilization, so ΔE_{AF}=-2J.

Since the J's are negative (i.e. antiferromagnetic coupling), for both complexes the $Fe^{III}NO^-$ configuration is stabilized by the increase in the number of its exchange pathways. The $Fe^{III}NO^-$ configuration is more stabilized in complex II by $\sim J_{AF}$ (see bottom of Scheme 3). This is qualitatively consistent with the above DFT calculations where complex II has an $Fe^{III}NO^-$ ground configuration, however this term is expected and calculated to be small ($\sim$ 0.14 eV).[68-71]

2) ΔE_{repl}—In going from the $Fe^{III}NO^-$ to the Fe^{II}-NO• configuration for both complexes in scheme 3, electron repulsion on the NO moiety is lost while the e^--e^- repulsion on the Fe is increased. For $\Delta E_{repl,NO}$, the NO^- loses $J(\pi_v^*, \pi_h^*) - K(\pi_v^*, \pi_h^*)$ repulsion, where J is the two electron Coulomb and K the two electron exchange integral. For $\Delta E_{repl,Fe}$, this change in e^--e^- repulsion must be obtained for each of the two configurations (for complex II: Fe^{III}(S=3/2) and Fe^{II}(S=1); for complex II + axial L: Fe^{III}(S=1/2) and Fe^{II}(S=0)) in terms of J and K integrals, which can be then rewritten in terms of the Racah parameters A, B, and C.[72, 73] These expressions are given in Table 3. The difference in the repulsion between the two configurations for each complex, ΔE_{repl}, is given at the bottom of Scheme 3. The first two terms, $\Delta E_{repl\ NO} + (15A_{Fe}^{II} - 10A_{Fe}^{III})$ are common in both and will be positive (i.e. favor the Fe^{III}-NO^- configuration) as the e^--e^- repulsion is higher on the metal iron than the NO. However, it is important to focus on the difference of the differences in configurational repulsion between the two complexes, equation 3.

$$\Delta\Delta E_{repl} = B_{Fe}^{II} + 7B_{Fe}^{III} - 3C_{Fe}^{II} + 5C_{Fe}^{III} \quad (3)$$

Since C_{Fe}^{III} is larger than C_{Fe}^{II}, this term is positive, indicating that the Fe^{III}-NO^-configuration is favored in complex II relative to complex II + axial L by this difference in electron repulsion. The magnitude of this term can be estimated from the Racah parameters. For Fe^{III}, B = 1015 cm^{-1}, C = 4800 cm^{-1}, and for Fe^{II}, B = 917 cm^{-1}, C = 4040 cm^{-1}. Their nephelauxetic reductions due to covalency in π backbonding complexes are found to be β=0.65 (Fe^{III}), and β=0.4 (Fe^{II}).[74-76] These give a calculated estimate that the Fe^{III}-NO^- configuration is stabilized in complex II by 1.95 – 2.5 eV (depending on the nephelauxetic reduction) relative to this configuration in complex II + axial L due to differences in e^--e^- repulsion. From table 3 a significant contribution to this is the exchange

given by $K(d_{z2},d_{xz}) + K(d_{yz},d_{xz})$, estimated to be 1.1 – 1.7 eV (dependent on the covalent reduction of the B and C) only present for the electronic configurations for complex II.

In summary, the difference in energy between the two configurations of each complex is:

$$\Delta E_{\mathrm{tot}}+\Delta E_{\mathrm{orb}}+\Delta E_{\mathrm{AF}}+\Delta E_{\mathrm{repl}} \quad (4)$$

The orbital term favors the Fe^{II}-NO• configuration, while the antiferromagnetic coupling (which is small) and the change in e^--e^- repulsion favor the $Fe^{III}NO^-$ configuration. For complex II, the electron exchange for Fe^{III}(S=3/2) dominates and the ground configuration is $Fe^{III}NO^-$ with the LMCT excited state (corresponding to the Fe^{II}-NO• configuration) calculated to be at 1.8 eV higher energy from TD-DFT. For complex II + axial L, in the low spin Fe^{III}(S=1/2)NO^-(S=1) configuration the two electron exchange is eliminated and the ground configuration is found to be Fe^{II}-NO• with the MLCT excited state (i.e. $Fe^{III}NO^-$ configuration) calculated (from TD-DFT) to be at 1.3 eV.

Discussion

A. Ligand Field and two e^- Exchange

The range of electronic structure descriptions of $\{FeNO\}^7$ complexes [3, 6-8, 10, 11, 14-31] is at least partially due to the different ligand environments of the different complexes. Most $\{FeNO\}^7$ (S=1/2) species studied in the literature[7, 17-20] are described as Fe^{II}(S=0)-NO•(S=1/2) complexes. Interestingly, all such complexes are six coordinate. The complex of Franz et al.[24] is five coordinate and is described as Fe^{III}(S=3/2)-NO^-(S=1), consistent with complex II in the present study. The complex of Hauser et al.[21] is also described as Fe^{III}(S=3/2)-NO^-(S=1), but has an additional axial Cl^- ligand. However, Cl^- is a relatively weak field ligand and when replaced by a stronger carboxylate ligand, the resultant complex is described as Fe^{II}(S=0)-NO•(S=1/2)[20]. Praneeth et al.[18] and Radoń et al.[31] also found that the axial ligand affects the electronic structure of $\{FeNO\}^7$ species.

The electronic structure descriptions of complex I, complex II and complex II + axial L determined in this study are Fe^{III}(S=5/2)-NO^-(S=1), Fe^{III}(S=3/2)-NO^-(S=1) and Fe^{II}(S=0)-NO•(S=1/2), respectively. In going from complex I (S=3/2) to complex II (S=1/2), the equatorial ligand field becomes stronger. As a result, the high spin Fe^{III} in complex I becomes an intermediate spin Fe^{III} in complex II. Complex II still has significant stabilization of the Fe^{III}-NO^- electronic configuration relative to the Fe^{II}-NO• configuration and thus Fe^{III}-NO^- is the experimentally determined electronic structure description. When an axial ligand is computationally added to complex II, the 10Dq on the Fe^{III} becomes large enough to stabilize low spin Fe^{III} which, in turn, leads to electron transfer from the NO^- to the Fe. This electron transfer is due to the relatively low two-electron exchange stabilization of the low spin Fe^{III} (and the fairly limited antiferromagnetic exchange coupling between the Fe^{III} and the NO^- in the Fe^{III}(S=1/2)-NO^-(S=1) configuration). The NO π^* orbital is at higher energy relative to the redox active Fe d orbital and thus transfers an electron to reduce the Fe, leading to the Fe^{II}(S=0)-NO•(S=1/2) description of the ground state. In summary, the ligand field defines the spin state of the ferric center. This changes the electron exchange and thus the electron distribution over the $\{FeNO\}^7$ unit.

B. Extension to $\{FeO_2\}^8$ Systems

At least three electronic structure descriptions have been considered for $\{FeO_2\}^8$ (S=0) sites, such as in hemoglobin: the Pauling description Fe^{II}(S=0)-O_2(S=0)[77], the Weiss description Fe^{III}(S=1/2)-O_2^-(S=1/2)[78] and the McClure-Goddard description Fe^{II}(S=1)-O_2(S=1)[79, 80] (Scheme 4). The model developed here for $\{FeNO\}^7$ can be extended to $\{FeO_2\}^8$ complexes

to consider the contributions that would stabilize each configuration. Using the approach described in the Analysis section E, the contribution to the relative E_{orb}, E_{AF} and E_{repl} for the three descriptions of $\{FeO_2\}^8$ are listed in Table 4. For E_{orb}, the three descriptions follow the order: Pauling < McClure-Goddard < Weiss; for the antiferromagnetic coupling (E_{AF}), the order is: McClure-Goddard < Weiss < Pauling; for $E_{repl,\ O2}$ and $E_{repl,Fe}$, the orders, respectively, are: McClure-Goddard < Pauling < Weiss and Weiss < McClure-Goddard < Pauling. Since the Coulombic repulsion between electrons in Fe d orbitals is larger than that in O_2 π^* orbitals, the total E_{repl} follows the order: Weiss < McClure-Goddard < Pauling. The electronic distribution that has the lowest total energy is again determined by the net effect of $E_{tot} = E_{orb} + E_{AF} + E_{repl}$.

Compared with the Pauling description, the Weiss configuration is favored by $E_{repl,Fe}$ and E_{AF} but disfavored by $E_{repl,\ O2}$ and E_{orb} (Scheme 4, Table 4). In going from the Weiss to the Pauling configuration, the change in $E_{repl,\ Fe}$ is the same as $\Delta E_{repl,\ Fe}$ in going from Fe^{III}(S=1/2)-NO^-(S=1) to Fe^{II}(S=0)-NO•(S=1/2) for complex II + axial L (Scheme 3, Table 3). The change in E_{AF} ($-1.5J_{AF}$) is smaller than ΔE_{AF} for complex II + axial L ($-2\ J_{AF}$, Scheme 3), by $-0.5J_{AF}$ assuming similar J_{AF} values. The change in $E_{repl,\ O2}$ in going from Weiss to Pauling ($-2J(\pi_v^*, \pi_h^*)$) is larger in magnitude than $\Delta E_{repl,\ NO}$ ($-[J(\pi_v^*,\pi_h^*) - K(\pi_v^*,\pi_h^*)]$) by $J(\pi_v^*,\pi_h^*) + K(\pi_v^*,\pi_h^*)$, due to the extra electron in $\pi_h^*$and the lack of two electron exchange in O_2^- (S=1/2). The change in E_{orb} in going from the Weiss to the Pauling configuration is expected to be smaller in magnitude than ΔE_{orb} in $\{FeNO\}^7$ due to the higher electronegativity of the oxygen atom. Therefore, compared with the $\{FeNO\}^7$ complex II + axial L where the electronic structure of the ground configuration is defined above as Fe(II)-NO•, for the $\{FeO_2\}^8$ complex the Pauling description (Fe^{II}(S=0)-O_2(S=0)) is favored by the $E_{repl,\ O2}$ contribution (and a small contribution from E_{AF}) while the Weiss description is favored by the decreased E_{orb} contribution. To evaluate the resultant effects of these differences in e^--e^- repulsion, E_{AF} and relative ligand and metal orbital energies, we have also calculated complex II + axial L as an $\{FeO_2\}^8$ S=0 system in both the Pauling (Fe^{II}(S=0)O_2(S=0)) and Weiss (Fe^{III}(S=1/2)-O_2^-(S=1/2)) configurations. Since complex II + axial L is a computation model, we have also calculated complex I and complex II which have been studied experimentally above as $\{FeO_2\}^8$ systems to calibrate this approach. These results are given in supporting information (Figure S4) and show their ground electronic configurations to be Fe^{III}(S=5/2)O_2^-(S=1/2) for complex I and Fe^{III}(S=3/2)-O_2^-(S=1/2) for complex II, consistent with their corresponding $\{FeNO\}^7$ ground electronic structures. However, for complex II + axial L the $\{FeO_2\}^8$ S=0 complex is calculated to have a Weiss like Fe^{III}(S=1/2)O_2^-(S=1/2) ground configuration with the Fe^{II}(S=0)-O_2(S=0) configuration at 16 kcal/mol higher energy. This is in contrast to the $\{FeNO\}^7$ species in complex II + axial L, which has an (Fe^{II}(S=0)-NO•) ground configuration. Thus, the lower energy of the O_2 π^* valence orbitals appears to be the key feature in shifting from the Fe^{II}-NO• to an $Fe^{III}O_2^-$ ground state. In fact, calculations of an $\{FeNO\}^8$ model of complex II + axial L give a ground configuration of Fe^{II}(S=0)-NO^-(S=0).[81]

Since E_{orb} is strongly impacted by the ligand field of Fe and the E_{repl} and E_{AF} are affected by the covalent delocalization of the MOs which affect $2e^-$ repulsion and antiferromagnetic coupling, the resultant effect of this combination of contributions in specific cases, in particular oxy-hemoglobin and oxy-picket fence porphyrin[82], is best determined by experiment. The most recent computational study of oxy-myoglobin favors the Weiss description[83].

Supplementary Material

Refer to Web version on PubMed Central for supplementary material.

Acknowledgments

This research was supported by NIH GM40392 (E.I.S.), RO1 GM45881-18 (J.A.K.) and NSF CHE 01-11629 and 09-10679 (M.Y.D.). SSRL operations are supported by the Department of Energy, Office of Basic Energy Sciences. The SSRL Structural Molecular Biology Program is supported by the National Institutes of Health, National Center for Research Resources, Biomedical Technology Program, and by the Department of Energy, Office of Biological and Environmental Research. This publication was made possible by Grant Number 5 P41 RR001209 from the National Center for Research Resources (NCRR), a component of the National Institutes of Health (NIH). Its contents are solely the responsibility of the authors and do not necessarily represent the official view of NCRR or NIH. L.V.L. is supported by a Larry Yung Stanford Graduate Fellowship. Yang Ha is thanked for assistance in the revision of the manuscript.

References

1. Costas M, Mehn MP, Jensen MP, Que L. Chem Rev. 2004; 104:939–986. [PubMed: 14871146]
2. Solomon EI, Brunold TC, Davis MI, Kemsley JN, Lee SK, Lehnert N, Neese F, Skulan AJ, Yang YS, Zhou J. Chem Rev. 2000; 100:235–349. [PubMed: 11749238]
3. Schenk G, Pau MYM, Solomon EI. J Am Chem Soc. 2004; 126:505–515. [PubMed: 14719948]
4. Arciero DM, Orville AM, Lipscomb JD. J Biol Chem. 1985; 260:4035–4044. [PubMed: 2858486]
5. Chen VJ, Orville AM, Harpel MR, Frolik CA, Surerus KK, Munck E, Lipscomb JD. J Biol Chem. 1989; 264:21677–21681. [PubMed: 2557336]
6. Clay MD, Cosper CA, Jenney FE, Adams MWW, Johnson MK. Proc Natl Acad Sci USA. 2003; 100:3796–3801. [PubMed: 12655067]
7. Pierce BS, Gardner JD, Bailey LJ, Brunold TC, Fox BG. Biochemistry. 2007; 46:8569–8578. [PubMed: 17602574]
8. Brown CD, Neidig ML, Neibergall MB, Lipscomb JD, Solomon EI. J Am Chem Soc. 2007; 129:7427–7438. [PubMed: 17506560]
9. Tierney DL, Rocklin AM, Lipscomb JD, Que L, Hoffman BM. J Am Chem Soc. 2005; 127:7005–7013. [PubMed: 15884944]
10. Westre TE, Di Cicco A, Filipponi A, Natoli CR, Hedman B, Solomon EI, Hodgson KO. J Am Chem Soc. 1994; 116:6757–6768.
11. Brown CA, Pavlosky MA, Westre TE, Zhang Y, Hedman B, Hodgson KO, Solomon EI. J Am Chem Soc. 1995; 117:715–732.
12. Collman JP, Yang Y, Dey A, Decreau RA, Ghosh S, Ohta T, Solomon EI. Proc Natl Acad Sci USA. 2008; 105:15660–15665. [PubMed: 18838684]
13. Enemark JH, Feltham RD. Coord Chem Rev. 1974; 13:339–406.
14. Rodriguez JH, Xia YM, Debrunner PG. J Am Chem Soc. 1999; 121:7846–7863.
15. Zhang Y, Oldfield E. J Am Chem Soc. 2004; 126:9494–9495. [PubMed: 15291525]
16. Zilberberg I, Ruzankin SP, Malykhin S, Zhidomirov GM. Chem Phys Lett. 2004; 394:392–396.
17. Li M, Bonnet D, Bill E, Neese F, Weyhermüller T, Blum N, Sellman D, Wieghardt K. Inorg Chem. 2002; 41:3444–3456. [PubMed: 12079463]
18. Praneeth VKK, Nather C, Peters G, Lehnert N. Inorg Chem. 2006; 45:2795–2811. [PubMed: 16562937]
19. Wanner M, Scheiring T, Kaim W, Slep LD, Baraldo LM, Olabe JA, Zalis S, Baerends EJ. Inorg Chem. 2001; 40:5704–5707. [PubMed: 11599974]
20. Serres RG, Grapperhaus CA, Bothe E, Bill E, Weyhermüller T, Neese F, Wieghardt K. J Am Chem Soc. 2004; 126:5138–5153. [PubMed: 15099097]
21. Hauser C, Glaser T, Bill E, Weyhermüller T, Wieghardt K. J Am Chem Soc. 2000; 122:4352–4365.
22. Radoń M, Broclawik E, Pierloot K. J Phys Chem B. 2010; 114:1518–1528. [PubMed: 20047294]
23. Hopmann KH, Ghosh A, Noodleman L. Inorg Chem. 2009; 48:9155–9165. [PubMed: 19780615]
24. Franz KJ, Lippard SJ. J Am Chem Soc. 1999; 121:10504–10512.
25. Conradie J, Quarless DA, Hsu HF, Harrop TC, Lippard SJ, Koch SA, Ghosh A. J Am Chem Soc. 2007; 129:10446–10456. [PubMed: 17685516]

26. Conradie J, Ghosh A. J Inorg Biochem. 2006; 100:2069–2073. [PubMed: 17081612]
27. Tangen E, Conradie J, Ghosh A. Inorg Chem. 2005; 44:8699–8706. [PubMed: 16296823]
28. Copik AJ, Waterson S, Swierczek SI, Bennett B, Holz RC. Inorg Chem. 2005; 44:1160–1162. [PubMed: 15732944]
29. Wanat A, Schneppensieper T, Stochel G, van Eldik R, Bill E, Wieghardt K. Inorg Chem. 2002; 41:4–10. [PubMed: 11782137]
30. Paulat F, Berto TC, George SD, Goodrich L, Praneeth VKK, Sulok CD, Lehnert N. Inorg Chem. 2008; 47:11449–11451. [PubMed: 18998631]
31. Radoń M, Pierloot K. J Phys Chem A. 2008; 112:11824–11832. [PubMed: 18942804]
32. Hedman B, Hodgson KO, Solomon EI. J Am Chem Soc. 1990; 112:1643–1645.
33. Glaser T, Hedman B, Hodgson KO, Solomon EI. Acc Chem Res. 2000; 33:859–868. [PubMed: 11123885]
34. Solomon EI, Hedman B, Hodgson KO, Dey A, Szilagyi RK. Coord Chem Rev. 2005; 249:97–129.
35. Neese F, Hedman B, Hodgson KO, Solomon EI. Inorg Chem. 1999; 38:4854–4860. [PubMed: 11671216]
36. Dey A, Chow M, Taniguchi K, Lugo-Mas P, Davin S, Maeda M, Kovacs JA, Odaka M, Hodgson KO, Hedman B, Solomon EI. J Am Chem Soc. 2006; 128:533–541. [PubMed: 16402841]
37. Kovacs, J. A., *Submitted*.
38. Chiang CY, Miller ML, Reibenspies JH, Darensbourg MY. J Am Chem Soc. 2004; 126:10867–10874. [PubMed: 15339171]
39. Shearer J, Nehring J, Lovell S, Kaminsky W, Kovacs JA. Inorg Chem. 2001; 40:5483–5484. [PubMed: 11599942]
40. Shearer J, Scarrow RC, Kovacs JA. J Am Chem Soc. 2002; 124:11709–11717. [PubMed: 12296737]
41. George, GN. EXAFSPAK and EDG_FIT. Stanford Synchrotron Radiation Laboratory, Stanford Linear Accelerator Center, Stanford University; Stanford, CA: 2000.
42. Tenderholt AL. PySpline, Version 1.0. http://pyspline.sourceforge.net/
43. Hedman B, Frank P, Gheller SF, Roe AL, Newton WE, Hodgson KO. J Am Chem Soc. 1988; 110:3798–3805.
44. Frisch, MJ., et al. Gaussian 03, Revision C.02. Gaussian, Inc.; Wallingford CT: 2004.
45. Becke AD. J Chem Phys. 1993; 98:5648–5652.
46. Lee CT, Yang WT, Parr RG. Phys Rev B. 1988; 37:785–789.
47. For complex I, a larger basis set was required to reproduce its experimental geometry.
48. Mulliken RS. J Chem Phys. 1955; 23:2338–2342.
49. Mulliken RS. J Chem Phys. 1955; 23:2343–2346.
50. Mulliken RS. J Chem Phys. 1955; 23:1833–1840.
51. Mulliken RS. J Chem Phys. 1955; 23:1841–1846.
52. Tenderholt AL. QMForge, Version 2.1. http://qmforge.sourceforge.net
53. Neese F, Olbrich G. Chem PhysLett. 2002; 362:170–178.
54. Neese F. ORCA – An Ab-initio, DFT and Semiempirical Electronic Structure Package, Version 2.6. 2008
55. Frisch, MJ., et al. Gaussian 09, Revision A.02. Gaussian, Inc.; Wallingford CT: 2009.
56. Münck, E.; Kovacs, J. A., et al. Unpublished results.
57. Westre TE, Kennepohl P, DeWitt JG, Hedman B, Hodgson KO, Solomon EI. J Am Chem Soc. 1997; 119:6297–6314.
58. Dey A, Jenney FE, Adams MWW, Johnson MK, Hodgson KO, Hedman B, Solomon EI. J Am Chem Soc. 2007; 129:12418–12431. [PubMed: 17887751]
59. Slater JC. Phys Rev. 1930; 36:0057–0064.
60. Note that the ligand field (LF) also affects the pre-edge transition energies, but to a smaller extent relative to Z_{eff}. The oxidation states derived here do not include the effect of the LF.
61. Zener C. Phys Rev. 1930; 36:0051–0056.

62. Unoccupied orbitals are used here to visualize the uncompensated occupied orbitals of opposite spin, which are strongly mixed due to spin polarization.
63. The results for the pure functional BP86 are not presented because they do not reproduce the energy splitting and the intensity pattern of the pre-edge in the S K-edge XAS.
64. George SD, Petrenko T, Neese F. Inorg Chim Acta. 2008; 361:965–972.
65. The transition to d_{x2-y2} (α) is lower in energy than transition to d_{x2-y2} (β) due to exchange stabilization of the quintet final state on the Fe.
66. Note that while the net charge donation from NO to Fe is larger in complex I (∼58%) than in complex II (∼45%), the NPA charge for complex I (1.8) is higher than complex II (1.5) due to differences in donation from the other ligands. This is consistent with the oxidation states estimated from the S K-edge energies in Supporting Information.
67. The energy difference between d_{x2-y2} and d_{xy} in complex II is not directly obtained because d_{x2-y2} and d_{xy} differ in occupancy. So a single point calculation on the complex II structure with a total spin S=3/2 was performed and the enery gap was obtained for the unoccupied d_{x2-y2} and d_{xy} orbitals.
68. This J was calculated for complex II using the broken-symmetry formalism of Noodleman[69,70] and Yamaguchi[71] (Scheme 3 left Fe^{III}-NO^{-} configuration). This has two strong magnetic orbital pathways out of six total, Complex II + axial L (Scheme 3 right Fe^{III}-NO^{-} configuration) has one strong magnetic pathway out of two total. Thus the J of Complex II + axial L should be ∼3/2 that of complex II. However, the stabilization energy due to the antiferromagnetic coupling of complex II should be ∼3/2 that of complex II + axial L (ΔE_{AF}'s at bottom of Scheme 3).
69. Noodleman L, Davidson ER. Chemical Physics. 1986; 109:131–143.
70. Noodleman L. J Chem Phys. 1981; 74:5737–5743.
71. Soda T, Kitagawa Y, Onishi T, Takano Y, Shigeta Y, Nagao H, Yoshioka Y, Yamaguchi K. Chem Phys Lett. 2000; 319:223–230.
72. Js and Ks are substituted by Racah parameters A, B and C using $J(d_{z2}, d_{xz}) = J(d_{z2}, d_{yz}) = A+2B + C$; $J(d_{z2}, d_{xy}) = A-4B + C$; $J(d_{yz}, d_{xz}) = J(d_{yz}, d_{xy}) = J(d_{xz}, d_{xy}) = A-2B + C$; $J(d_{xz}, d_{xz}) = J(d_{yz}, d_{yz}) = J(d_{xy}, d_{xy}) = A+4B+3C$; $K(d_{z2}, d_{xz}) = K(d_{z2}, d_{yz}) = B + C$; $K(d_{yz}, d_{xz}) = 3B + C$.
73. Sugano, S.; Tanabe, Y.; Kamimura, H. Multiplets of transition-metal ions in crystals. Academic; New York: 1970.
74. Figgis, BN.; Hitchman, MA. Ligand field theory and its applications. Wiley-VCH; 2000.
75. Naiman CS. J Chem Phys. 1961; 35:323–328.
76. The values used for β are the experimental values for $K_3[Fe(CN)_6]$ and $K_4[Fe(CN)_6]$, which have π back-bonding as in the FeNO complexes.
77. Pauling L, Weiss JJ. Nature. 1964; 203:182–183. [PubMed: 14207238]
78. Weiss JJ. Nature. 1964; 202:83–84. [PubMed: 14166723]
79. McClure DS. Radiation Res Suppl. 1960; 2:218.
80. Goddard WA, Olafson BD. Proc Natl Acad Sci USA. 1975; 72:2335–2339. [PubMed: 1056005]
81. Compared with the Pauling description, the McClure-Goddard configuration is favored by $E_{repl, Fe}$, and E_{AF} but disfavored by E_{orb} (Table 4). The difference in E_{AF} is $-4J_{AF}$ ∼0.5 eV. Using the A, B, C expressions of Fe^{II} (S=1, as in complex II) and Fe^{II} (S=0, as in complex II + axial L) (Table 3), the difference in $E_{repl,Fe}$ is estimated to be −B + 3C = ∼1 eV dependent on nephelauxetic reduction (see Analysis section E). The difference in $E_{repl,Fe}$ is estimated to be ∼1 eV from the singlet-triplet energy gap in O_2. The difference in E_{orb} between the Pauling and the McClure-Goddard descriptions is the energy splitting of the O_2 π_h^* and π_v^* orbitals plus the energy splitting between d_{yz} and d_z^2 which is determined by the specific ligand field of the Fe center. Therefore, the contributions from $E_{repl,Fe}$, and E_{AF} favor the McClure-Goddard description by ∼2.5 eV, which is offset by the energy splitting between the O_2 π_h^* and π_v^* orbitals (dependent on the strength of the O_2-Fe bond) plus the energy splitting of Fe d_{yz} and d_z^2 orbitals (dependent on the ligand field of the Fe).
82. Collman JP, Gagne RR, Gray HB, Hare JW. J Am Chem Soc. 1974; 96:6522–6524.
83. Chen H, Ikeda-Saito M, Shaik S. J Am Chem Soc. 2008; 130:14778–14790. [PubMed: 18847206]

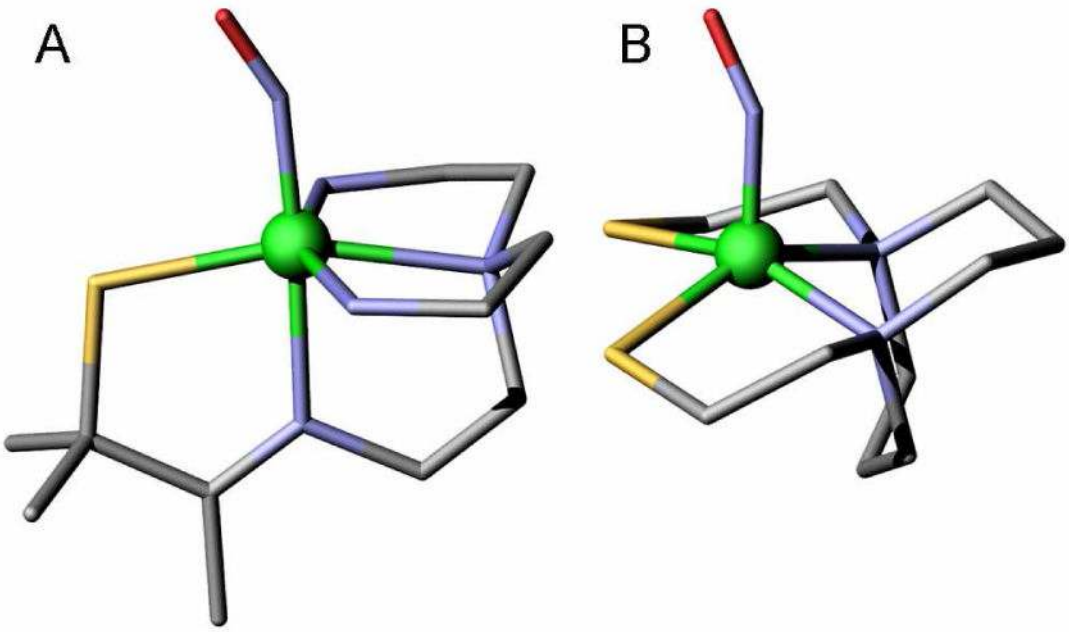

Figure 1.
Molecular structures of A) complex I and B) complex II, from x-ray crystallography[37,38]. (Fe atoms are in green, S atoms are in yellow, C atoms are in grey, and N atoms are in blue. H atoms are omitted for clearity).

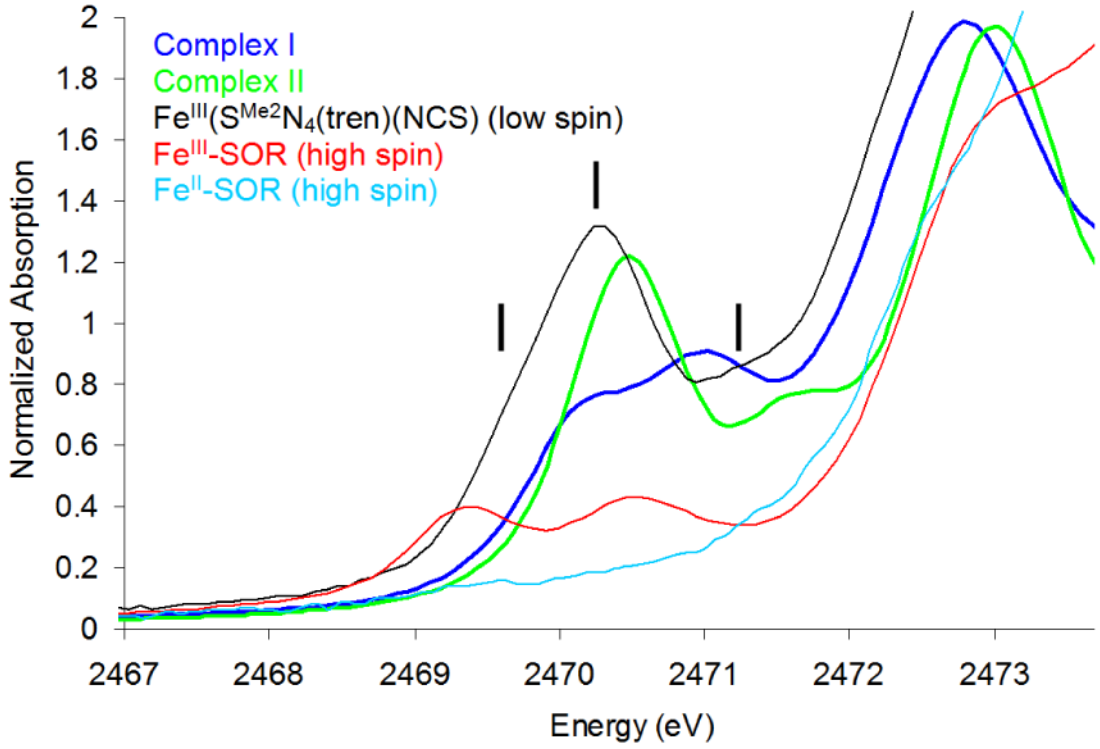

Figure 2.

S K-edge XAS spectra of complex I ({FeNO}^{7}, S=3/2, blue), complex II ({FeNO}^{7}, S=1/2, green), Fe^{III}-SOR (high spin, red), $Fe^{III}(S^{Me2}N_4(tren))(NCS)$ (low spin, black) and Fe^{II}-SOR (high spin, light blue). The vertical lines indicate the three pre-edge features associated with transitions to $^1A_1$, to $^3T_1$, $^3T_2$ and $^1T_1$, and to $^1T_2$ states for $Fe^{III}(S^{Me2}N_4(tren))(NCS)$.

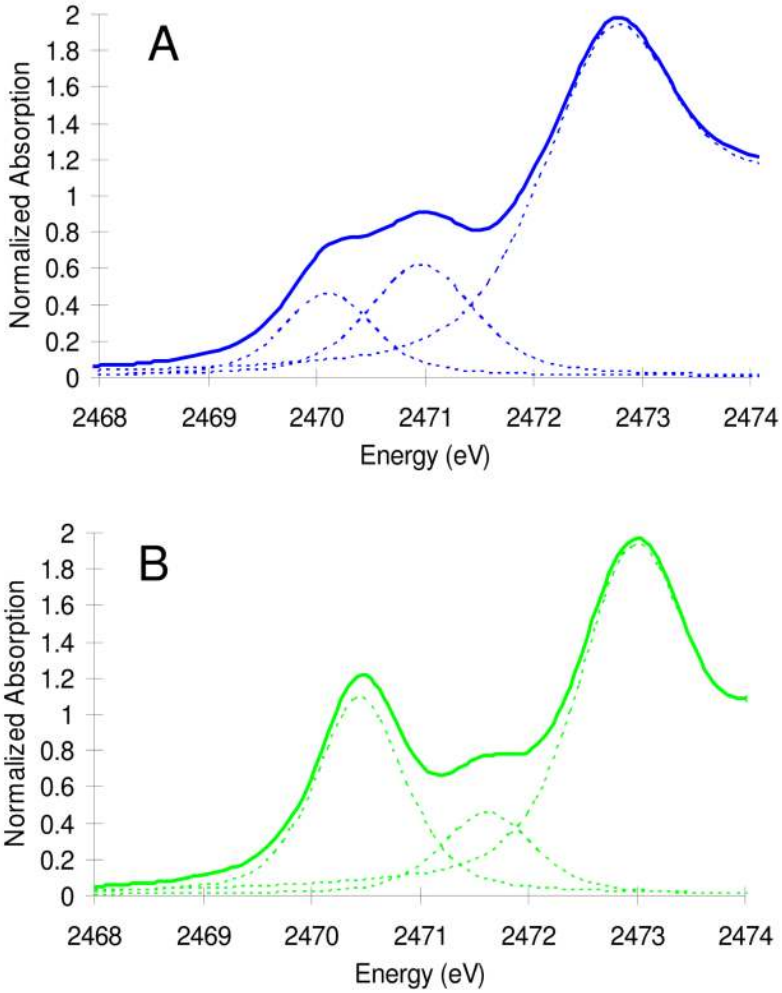

Figure 3.
Fits of the pre-edge features of complex I (A) and complex II (B).

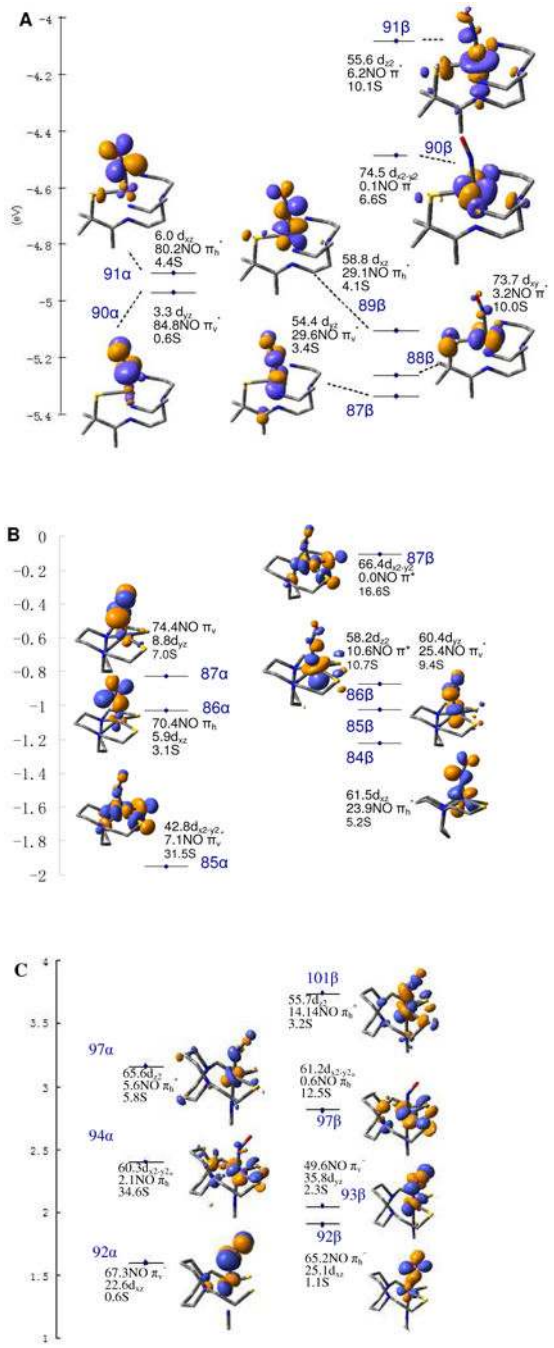

Figure 4.

MO diagrams of complex I (A), complex II (B) and complex II + axial L (C). (Only unoccupied orbitals are shown. Occupied orbitals are in Figure S1-S3.) Numbers shown are the percentage of Fe d, NO_{2p} and S_{3p} orbitals in each MO. α contours are shown on the left and β contours on the right.

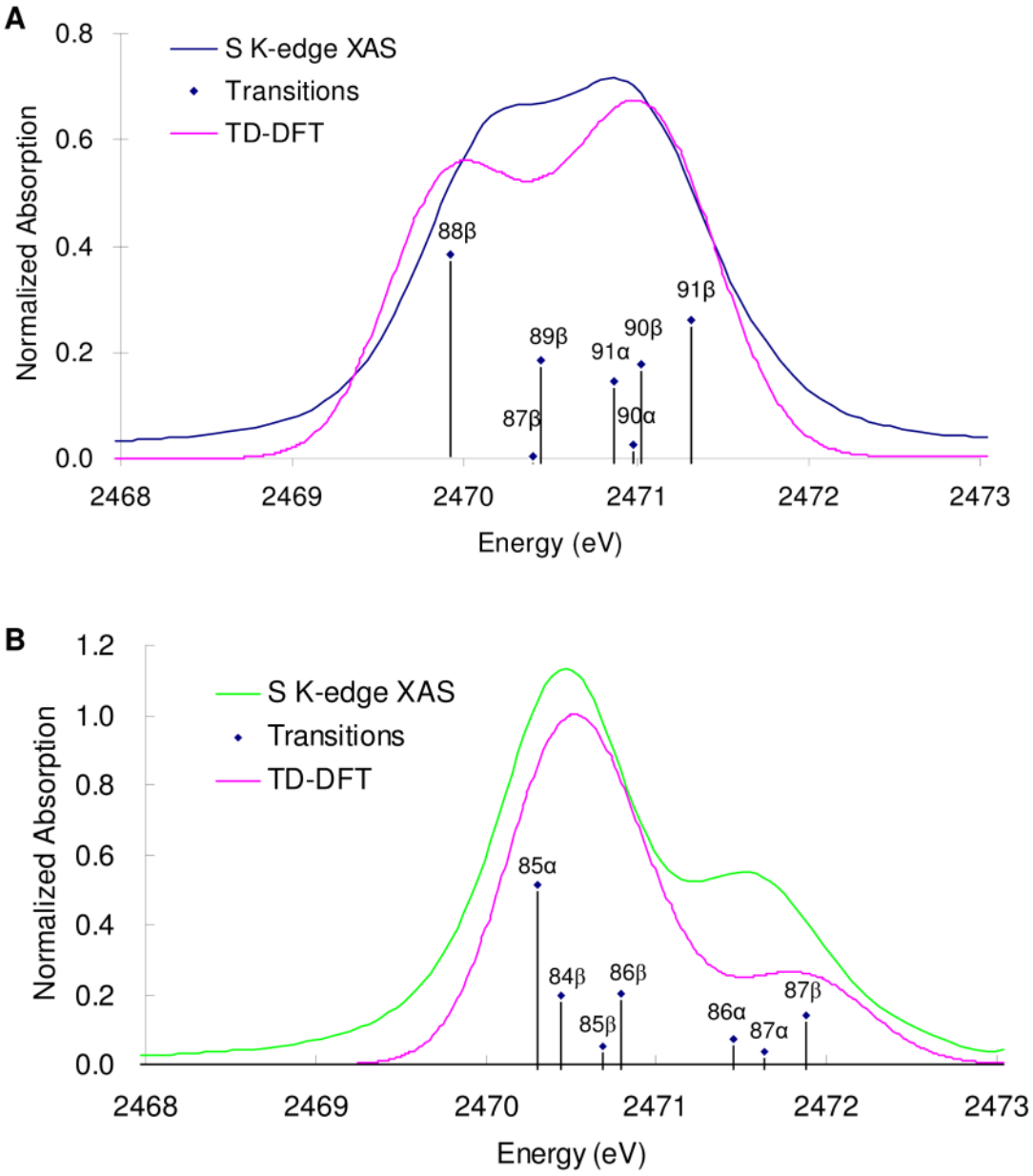

Figure 5.
TD-DFT calculated (pink) and experimental (blue for complex I and green for complex II) S K-edge XAS spectra for complex I (A) and complex II (B). The transitions have been convolved with a pseudo-Voigt function of 0.5 eV half-width to account for experimental and core-hole broadening.

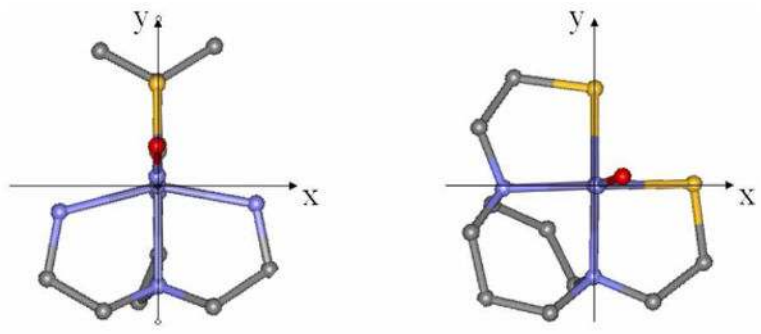

Figure 6.
Equatorial ligand field of complex I (left) and complex II (right). Note complex II has two strongly donating *cis* thiolates and four equal L-Fe-L angles (L=S or N) of 86(±2)° while complex I has one thiolate, two N-Fe-N angles of 53° and two S-Fe-N angles of 101°.

Fe(II) - NO·		Fe(III) – NO^-		Fe(I) – NO^+	
S=2	S=1/2	S=5/2	S=1	S=3/2	S=0
S=1	S=1/2	S=1/2	S=1		
		S=3/2	S=0		

Fe(II) - NO·		Fe(III) – NO^-		Fe(I) – NO^+	
S=1	S=1/2	S=3/2	S=1	S=1/2	S=0
S=0	S=1/2	S=1/2	S=1		
		S=1/2	S=0		

Scheme 1.
Scheme 1A. Plausible descriptions of $\{FeNO\}^7$ S=3/2 spin states.
Scheme 1B. Plausible descriptions of $\{FeNO\}^7$ S=1/2 spin states.

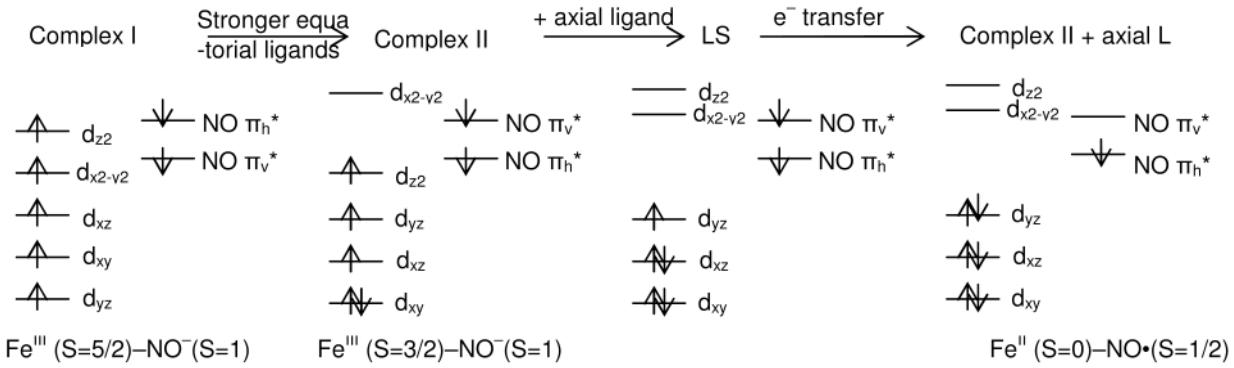

Scheme 2.
Descriptions of $\{FeNO\}^7$ complexes with different ligand fields.

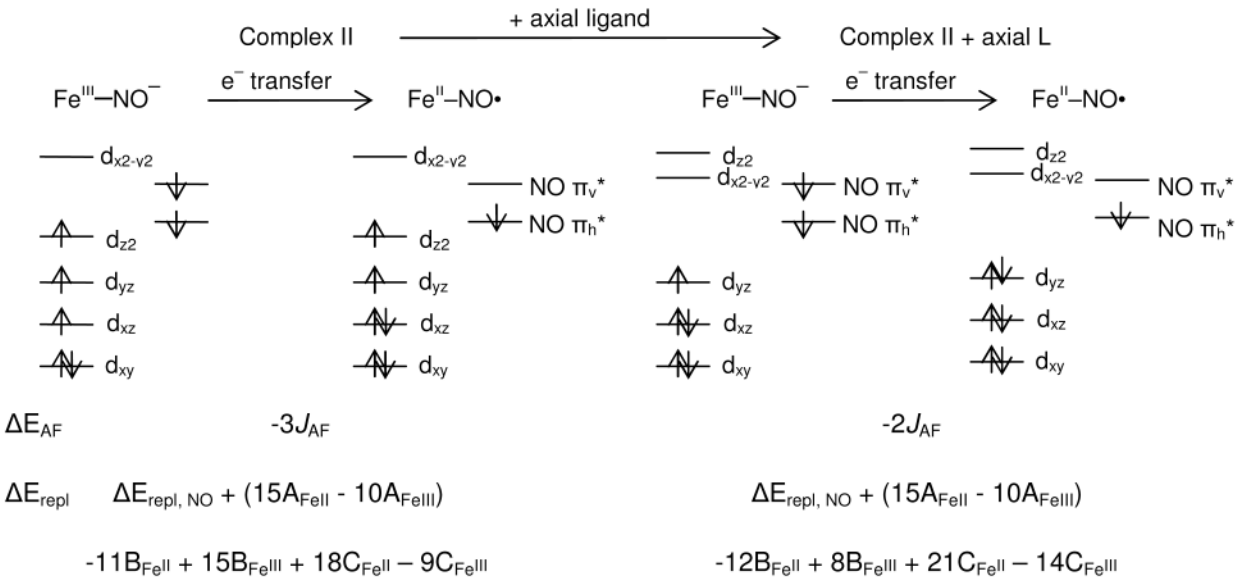

Scheme 3.

Correlation between descriptions for complex II and complex II + axial L (contributions to energy difference between Fe^{III}–NO^{-} and Fe^{II}–NO• for each complex at bottom).

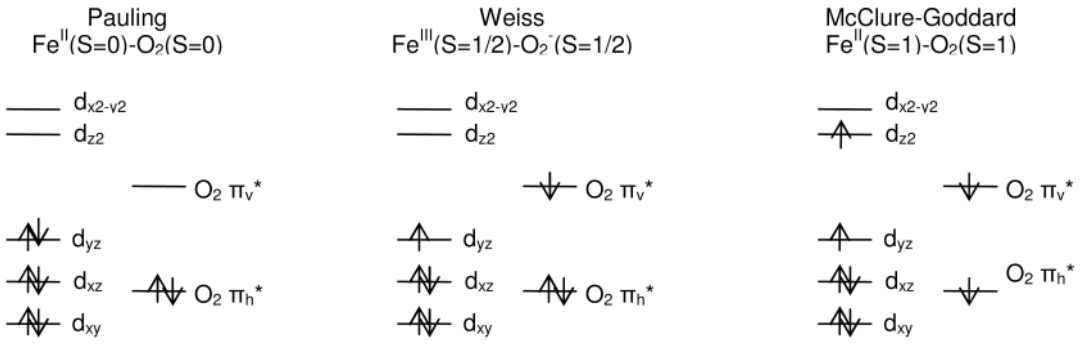

Scheme 4.
Three electronic structure descriptions of $\{FeO_2\}^8$

Table 1

Geometric parameters, spin densities, and S covalencies from crystal structures, experimental data, and calculations.

Fe(trenS)NO (complex I)			**Fe(daco)NO (complex II)**		
	Exp.	**B3LYP**		**Exp.**	**B3LYP**
Fe-S	2.28	2.28	Fe-S1	2.24	2.26
Fe-N1	2.12	2.21	Fe-S2	2.25	2.26
Fe-N3	2.2	2.34	Fe-N1	2.07	2.15
Fe-N2A	2.21	2.32	Fe-N2	2.08	2.15
Fe-N2B	2.21	2.29			
Fe-NO	1.76	1.8	Fe-NO	1.70	1.73
N-O	1.15	1.16	N-O	1.17	1.19
Fe-N-O	152.6	161	Fe-N-O	151.4	149.8
O-N-Fe-S	0	-14.3	O-N-Fe-S1	20.3	46
Spin density on Fe		3.67	Spin density on Fe		2.16
Spin density on NO		-1.13	Spin density on NO		-1.15
S covalency	43 [a]	39	S covalency	55 [a]	40

[a] From the covalency in Table 2.

Table 2

Pre-edge peak energies (E, eV), intensities (D_0) and covalencies.

Complex	*E* (eV)	D_0	Covalency[a]	Total covalency
I	2470.1	0.44	17	43
	2471.0	0.70	26	
II	2470.5	1.05	39	55
	2471.6	0.42	16	

[a]Quantitation was based on the expression $D_0 = A\alpha^2 I(S)/3n$, where α^2 is the S character in each orbital, A is the ground state degeneracy, *n* is the normalization factor (i.e., number of S atoms contributing to the pre-edge feature, *n*=1 for complex I and *n*=2 for complex II) and *I(S)* is the transition dipole integral (*I(S)*=8.05 for thiolate[34]).

Table 3

$E_{repl,\ Fe}$ for complex II and for complex II + axial L in terms of Coulomb, and exchange integrals, and their conversion to Racah parameters.

		Expressions in J and K	Expressions in A, B and C
Complex II	Fe^{III}	$J(d_{z2}, d_{yz}) + J(d_{z2}, d_{xz}) + 2J(d_{z2}, d_{xy}) + J(d_{yz}, d_{xz}) + 2J(d_{yz}, d_{xy}) + 2J(d_{xz}, d_{xy}) + J(d_{xy}, d_{xy}) - K(d_{z2}, d_{yz}) - K(d_{z2}, d_{xz}) - K(d_{yz}, d_{xz})$	10A−15B+9C
	Fe^{II}	$J(d_{z2}, d_{yz}) + 2J(d_{z2}, d_{xz}) + 2J(d_{z2}, d_{xy}) + 2J(d_{yz}, d_{xz}) + 2J(d_{yz}, d_{xy}) + J(d_{xz}, d_{xz}) + 4J(d_{xz}, d_{xy}) + J(d_{xy}, d_{xy}) - K(d_{z2}, d_{yz})$	15A−11B+18C
Complex II + axial L	Fe^{III}	$2J(d_{yz}, d_{xz}) + 2J(d_{yz}, d_{xy}) + J(d_{xz}, d_{xz}) + 4J(d_{xz}, d_{xy}) + J(d_{xy}, d_{xy})$	10A−8B+14C
	Fe^{II}	$J(d_{yz}, d_{yz}) + 4J(d_{yz}, d_{xz}) + 4J(d_{yz}, d_{xy}) + J(d_{xz}, d_{xz}) + 4J(d_{xz}, d_{xy}) + J(d_{xy}, d_{xy})$	15A−12B+21C

Table 4

Expressions of relative E_{orb}, E_{repl} and E_{AF} for the three descriptions of $\{FeO_2\}^8$

	Pauling	Weiss	McClure-Goddard
E_{orb}[1]	0	$E_{\pi_v^*} - E_{d_{yz}}$	$E_{d_{z2}} - E_{d_{yz}} + E_{\pi_v^*} - E_{\pi_h^*}$
E_{AF}	0	$-3/2J_{AF}$	$-4J_{AF}$
$E_{repl,Fe}$	$J(d_{yz},d_{yz}) + 4J(d_{yz},d_{xz}) + 4J(d_{yz},d_{xy}) + J(d_{xz},d_{xz}) + 4\ J(d_{xz},d_{xy}) + J(d_{xy},d_{xy})$	$2J(d_{yz},d_{xz}) + 2J(d_{yz},d_{xy}) + J(d_{xz},d_{xz}) + 4\ J(d_{xz},d_{xy}) + J(d_{xy},d_{xy})$	$J(d_{z2},d_{yz}) + 2J(d_{z2},d_{xz}) + 2J(d_{z2},d_{xy}) + 2J(d_{yz},d_{xz}) + 2J(d_{yz},d_{xy}) + J(d_{xz},d_{xz}) + 4\ J(d_{xz},d_{xy}) + J(d_{xy},d_{xy}) - K(d_{z2},d_{yz})$
E_{repl}			
$E_{repl,O2}$	$J(\pi_h^*, \pi_h^*)$	$J(\pi_h^*, \pi_h^*) + 2J(\pi_v^*, \pi_h^*)$	$J(\pi_v^*, \pi_h^*) - K(\pi_v^*, \pi_h^*)$

[1] E_{Orb} (Pauling) defined as 0.